Research on Electromagnetic Shielding Effectiveness of Multi-layered LZ91/Al Alloy Composite Materials by Asynchronous Accumulative Roll Bonding

Tongying ZHANG [1], Hao HU [1], Junli WANG [2]*, Zhongxue FEN [1], Jiewen GUO [1], Xueliang LIU [1]

[1] *Institute of Materials Science and Engineering, Kunming University of Science and Technology, Kunming, 650093, China*
[2] *Research Center for Analysis and Measurement, Kunming University of Science and Technology, Kunming 650093, China*

crossref http://dx.doi.org/10.5755/j02.ms.29571

Received 17 August 2021; accepted 21 December 2021

In this paper, the multi-layered LZ91/Al alloy composite materials were prepared by asynchronous accumulative roll bonding (AARB), and the effect of the multilayer structure on the electromagnetic shielding effectiveness of the alloy was investigated. The result show that the number of LZ91 and Al layers increase exponentially with the increase of AARB passes, and the LZ91 layer and Al layer, α-Mg phase and β-Li phase in the alloy are arranged alternately. Besides, as the aggregate thickness of the Al layer increases in the AARB process, the electrical conductivity of the alloy also increases. Thish can effectively improve the electromagnetic shielding effectiveness of the alloy.
Keywords: asynchronous accumulative roll bonding, LZ91 alloy, multi-layered LZ91/Al alloy composite materials, electromagnetic shielding.

1. INTRODUCTION

With the popularization of 5G communication technology and the extensive use of electronic equipment, it will bring many electromagnetic waves to people's daily lives, leading to increasingly serious electromagnetic pollution [1]. Electromagnetic pollution not only affects the natural environment and human health [2, 3], but also affects the normal operation of electronic equipment [4]. Especially in aerospace [5], electromagnetic interference can affect the communication command and control system, resulting in danger and accidents. Even in the military [6], the leakage of the electromagnetic wave will cause the disclosure of secrets, threatening national security. Therefore, the research and development of electromagnetic shielding materials have become an important topic in the field of materials research.

At present, the research on electromagnetic shielding effectiveness is widely based on the transmission line model. Schelkunoff used Maxwell equations and TL Model to derive its mathematical expression [7]. It can be seen the shielding effectiveness (*SE*) depends on the three following mechanisms from Eq. 1 – Eq. 4: reflection loss (SE_R), absorption loss (SE_A), and multiple reflection loss (SE_B). SE_R refers to the loss when the electromagnetic wave passes through the medium with inconsistent impedance, and its value is only related to the characteristic impedance of the material; SE_A refers to the attenuation of the electromagnetic wave when it passes through the medium, and its value depends on the thickness, the electrical conductivity and the magnetic permeability of the material; SE_B refers to the loss caused by multiple reflection of the electromagnetic wave at the internal interface of the medium, its value depends on the uniformity of the internal structure of the material.

$$SE = \frac{1}{p}(1 - qe^{-2\gamma t_s})e^{\gamma t_s}; \quad (1)$$

$$SE_A = 20\log_{10}\left(e^{\frac{t_s}{\delta_s}}\right) = 8.686\left(\frac{t_s}{\delta_s}\right); \quad (2)$$

$$SE_R = 20\log_{10}\frac{1}{p} = 20\log_{10}\frac{|1+k|^2}{4|k|}; \quad (3)$$

$$SE_B = 20\log_{10}\left(1 - qe^{\frac{-2t_s}{\delta_s}}\right) = 20\log_{10}\left|1 - \frac{(k-1)^2}{(k+1)^2}e^{\frac{-2t_s}{\delta_s}}\right|, \quad (4)$$

where γ is the propagation vector; $\gamma = \alpha + j\beta$, β is the displacement vector; α is the attenuation vector, $\alpha = \beta = \sqrt{\pi\mu f\sigma} = \frac{1}{\delta_s}$. δ_s(in m) is the skin depth; f(in Hz) is the electromagnetic radiation frequency; $k = \frac{Z_S}{Z_0}$, Z_s(in Ω) is the characteristic impedance; $Z_s = \sqrt{\frac{j\omega\mu_s}{\sigma_s}}$; Z_0 is the characteristic impedance of air; $Z_0 = 377\ \Omega$; t_s(in m) is the thickness. μ_s(in H/m) is the magnetic permeability; σ_s(in S/m) is the electrical conductivity.

Mg alloy has the advantages of low density, high specific strength, high damping, good cutting and excellent electromagnetic shielding properties [8], so it has excellent application prospects in both aerospace and electromagnetic shielding fields. And in the research of electromagnetic shielding properties of magnesium alloy, Liu Lizi et al. [9] studied the electromagnetic shielding effectiveness of as cast Mg-$_x$Zn-$_y$Y (x = 2~5 wt.%, y = 1~10 wt.%) alloy, and considered that the electrical conductivity decreased with the increase of Y/Zn ratio, which leads to the decrease of electromagnetic shielding effectiveness. The effect of texture on shielding effectiveness of Mg-Zn-Zr-Ce alloy was studied in [10]. Chen Xianhua et al. [11] studied the effect of heat treatment on electromagnetic shielding

* Corresponding author. Tel.: +86-871-65916005.
E-mail address: *20070141@kust.edu.cn* (J. Wang)

effectiveness of ZK60 alloy and considered that the precipitation of solute elements is conducive to improving the electromagnetic shielding effectiveness. Wang Jiahao et al. [12] studied the effect of cross interaction of dual-phase on electromagnetic shielding effectiveness of Mg-9Li alloy during different rolling stain. Xu Zhichao et al. [13] studied the influence of directional solidification on the electromagnetic shielding effectiveness of Mg-Zn-Y alloy by controlling the orientation relationship between the LPSO phase and matrix. In conclusion, the research on electromagnetic shielding effectiveness of Mg alloys mainly focuses on: (1) SE_A and SE_R can be improved by changing the alloy element ratio and heat treatment; (2) SE_R can be improved by deformation texture; (3) changing the grain boundary density, phase boundary density and the orientation relationship between phase and matrix improves SE_B. Schulz R.B. et al. [14] established a multi-layered shielding model and theoretically pointed out its feasibility. However, the research on this multi-layered structure magnesium alloy is rare, which needs further research and analysis.

Accumulative Rolling Bonding (ARB) [15] is a severe plastic deformation process with the characteristics of superimposed rolling and repeated deformation, which can not only realize the preparation of multi-layer materials but also prepare ultra-fine grained materials with excellent performance due to a large amount of deformation. AARB [16] is a new process that introduces asynchronous rolling into ARB, which combines the advantages of both. Compared with ARB, AARB can produce additional shear deformation in the rolling process, thus further improving the mechanical properties of materials. Mg-Li alloy is a special magnesium alloy with ultra-light properties. According to the binary phase diagram of Mg-Li alloy [17], when the Li content is between 5.3 wt.% and 10.7 wt.%, the alloy shows a typical dual-phase structure, so it also has obvious advantages in electromagnetic shielding. When Al alloy is coated on Mg alloy, its plasticity and corrosion resistance can be improved through the complementary effects of various materials [18], and the addition of Al layer can improve the electrical conductivity of the material, which is similar to conductive coating materials [19]. Moreover, Al alloy and Mg alloy are both light metals, which will not deteriorate the shielding density of multi-layered composite materials [20], in addition, the addition of the Al layer increases the number of alloy layers, strengthens the interface reflection, and is also conducive to electromagnetic shielding effectiveness.

In this paper, LZ91 alloy and industrial pure aluminum alloy were used as the original materials. And LZ91/Al composite matetial, a multi-layered structural material formed by the alternating arrangement of Al/Mg/Al/Mg/...../Al, is prepared by AARB. Its electromagnetic shielding effectiveness was studied from experiment and theoretical arithmetic.

2. EXPERIMENT

The experimental materials were LZ91 magnesium alloy and 1070 industrial pure aluminum (≥ 99.9 wt.%). The thickness of 1070 Al alloy was 0.015 mm. The LZ91 alloy was annealed state and provided by Zhengzhou Institute of light metals of Chinalco with the thickness of 0.54 mm, and its chemical composition is shown in Table 1.

Table 1. Chemical composition of LZ91 alloy, wt.%

Element	Li	Zn	Mg	Other
Content	9.05	1.05	89.82	Bal.

Cut the LZ91 alloy strip into a specimen of 60 mm × 35 mm × 0.5 mm by wire cutting. Polished the specimen with a wire brush until it was bright to remove the oxide layer on the surface, and then cleaned the surface with acetone to remove the surface oil. Two surface-treated specimens were aligned from top to bottom, a layer of aluminum foil sandwiched between them, and riveted at both ends, coated the aluminum foil on the surface. The AARB experiment was carried out on the two-high asynchronous rolling mill LG-300, and the asynchronous ratio is 1:1.08. After that, the specimen was heated at 250 °C for 5 min in a box resistance furnace, and carried out the AARB experiment with 50 % reduction, then repeated the above steps for a total of 4 passes. Those specimens were named as $AARB_0$, $AARB_1$, $AARB_2$, $AARB_3$ and $AARB_4$, and $AARB_0$ was the original specimen, and the theoretical thicknesses of $AARB_0$ to $AARB_4$ are 0.54 mm, 0.562 mm, 0.577 mm, 0.594 mm, 0.607 mm, respectively. The microstructure was observed by Olympus Bx51m optical microscope, and the phase composition was analyzed by D/max-2200 X-ray diffraction. The Hall Effect Measurement System was used to test the electrical conductivity of specimens, carried out five measurements for each pass, and fetched the average as the electrical conductivity. The coaxial tester was used to test the electromagnetic shielding effectiveness, the test standard was ASTMD4935-2010, the measuring instrument was DR-S02 planar analogy shielding effectiveness tester, and the test frequency was 30 MHz~1.5 GHz.

3. RESULTS AND ANALYSIS

3.1. Microstructures

Fig. 1 shows the metallographic microstructure and XRD pattern of the LZ91 original state. It can be seen that LZ91 alloy is mainly composed of bcc Li_3Mg_7(β-Li) and hcp $Li_{0.92}Mg_{4.08}$(α-Mg). And in LZ91 alloy, α-Mg phase is about 30 %, β-Li phase is about 70 %, therefore, in Fig. 1, α-Mg phase is represented the white phase, and β-Li phase is represented the gray phase.

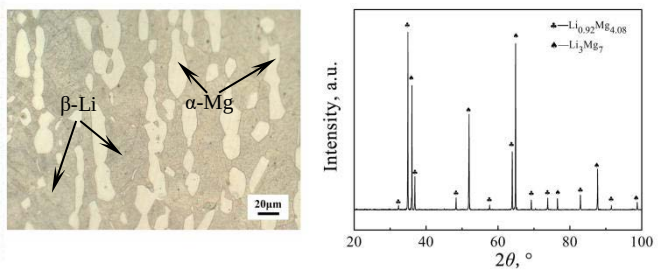

a b

Fig. 1. Microstructure of original state LZ91 alloy: a – metallography microstructure; b – XRD pattern

Fig. 2 shows the microstructure of LZ91/Al alloy under different AARB passes, it can be seen that LZ91/Al alloy is in the alternate arrangement of Al/Mg/Al/Mg/.../Al structure under AARB, and the interface between LZ91 and Al alloy is obvious and combines well. As can be seen from Fig. 2 a – Fig. 2 e, with the increase of rolling passes, the layer number of LZ91 alloy increases exponentaly as 2^n (n is the AARB pass), $AARB_1$ to $AARB_4$ is 2, 4, 8, 16, respectively. The layer thickness in ND decreases uniformly, and the average thickness of $AARB_1$ to $AARB_4$ is 267.41, 134.14, 63.13, 32.75 μm, respectively, the layer number of Al alloy varies as 2^n+1, the thickness of Al layer changes in a stripe code pattern because the fresh coating of aluminum foil before each pass, which is consistent with coded-ARB [21]. However, the total thickness of Al alloy increases, and the average thickness is respectively about 13.31, 6.69, 3.57, 2.67 μm from $AARB_1$ to $AARB_4$. Besides, from Fig. 1 and Fig. 2 f – Fig. 2 i), it can be seen that with the increase of passes, α-Mg and β-Li elongate along RD, refine and alternate along ND, and the phase spacing in ND decreases gradually, then α-Mg fracture and evenly distributes in LZ91 sheet, Of original LZ91 alloy α- Mg particles are relatively large, and the particle size is about 15 μm. Its thickness in ND is about 3~8 μm after $AARB_2$, and rapidly thinned to less than 3 μm by $AARB_4$, and most are maintained at about 1μm, which is due to the fact that the alloy is subjected to a great amount of deformation in the AARB process, and the accumulated deformation energy storage forces the grain refinement.

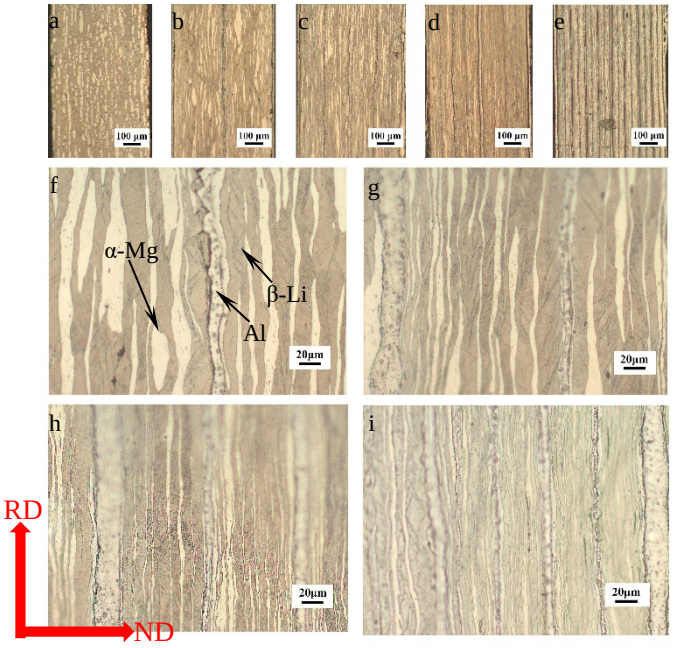

Fig. 2. Microstructure of LZ91/Al with different passes: a – $AARB_0$; b, f – $AARB_1$; c, g – $AARB_2$; d, h – $AARB_3$; e, i – $AARB_4$

3.2. Electromagnetic shielding effectiveness

Fig. 3 shows the electrical conductivity and the electromagnetic shielding effectiveness of multi-layered LZ91/Al composite materials with different passes. After plastic deformation, there are lots of dislocation entanglements in materials in general, which can increase the resistivity and decrease the electrical conductivity of the material. However, in this paper, the electrical conductivity of multi-layered LZ91/Al composite materials not only decreases with the increase of passes but also increases significantly as shown in Fig. 3 a. The cause of this phenomenon is traced back to the addition of the Al layer in each AARB pass. Assuming that the influence of rolling on the electrical conductivity of the alloy is ignored and the thickness of the material is approximately unchanged in the 50 % reduction, the electrical conductivity calculation formula of multi-layered LZ91/Al composite materials can be established according to the mixing rule [22], as shown in Eq. 5. In the equation, $\sigma_{Al} > \sigma_{LZ91}$, so the addition of Al layer can improve the electrical conductivity of the alloy. It is also known that the electrical conductivity of the alloy $\sigma_{LZ91/Al}$ also increases with increasing AARB passes due to the total thickness of the Al layer d_{Al} increases continuously. The electromagnetic shielding effectiveness of multi-layered LZ91/Al composite materials is among the most excellent, and their values are all greater than 100 dB, as shown in Fig. 3 b. It can also be found that the electromagnetic shielding effectiveness of the alloy generally increases with AARB passes, but the electromagnetic shielding effectiveness of $AARB_2$ is slightly lower than $AARB_1$ at about 1300 MHz~1500 MHz. And as known above the paper, the main factors that affect the electromagnetic shielding effectiveness are SE_A, SE_R, and SE_B. The SE_A is consistent with the changing trend of electrical conductivity, so it is consistent with the changing trend of Fig. 3 a. And the impedance between LZ91 and Al alloy is discontinuous, while the interface between heterogeneous metals increases sharply, the SE_R and SE_B have the same trend with it. In addition, there are also a large number of α-Mg/β-Li interfaces in the multi-layered LZ91/Al composite materials, which also intensifies the SE_R and SE_B. And the specific analysis of electromagnetic shielding effectiveness of LZ91/Al composite materials with different passes is shown below.

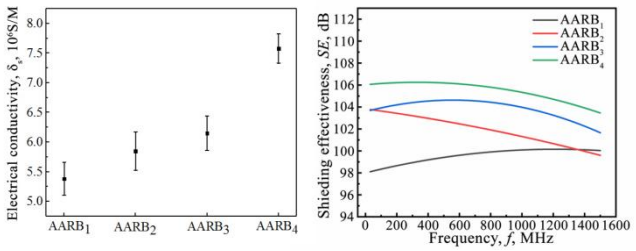

a b

Fig. 3. The electrical conductivity and the shielding properties of LZ91/Al alloy with different rolling passes: a – electrical conductivity; b – electromagnetic shielding effectiveness

$$\sigma_{LZ91/Al} = \frac{V_{LZ91}\sigma_{LZ91}+V_{Al}\sigma_{Al}}{V_{LZ91}+V_{Al}} = \frac{d_{LZ91}\sigma_{LZ91}+d_{Al}\sigma_{Al}}{d_{LZ91}+d_{Al}}. \quad (5)$$

3.3. Analysis and discussion

For multi-layered uniform model, its electromagnetic shielding effectiveness is shown in Eq. 6 – Eq. 10 [14]:

$$SE = 20\log_{10}\left|\frac{1}{P}\prod_{n=2}^{N-1} e^{j\boldsymbol{k}_{xnd_n}}\left(1 - q_n e^{-2j\boldsymbol{k}_{xnd_n}}\right)\right|; \quad (6)$$

$$P = \frac{2Z_0 \prod_{i=1}^{N-1} 2Z_i}{(Z_0+Z_1)\prod_{i=1}^{N-1}(Z_i+Z_{i+1})}; \quad (7)$$

$$q_i = \frac{(Z_i-Z_{i-1})(Z_i-Z_{i+1})}{(Z_i+Z_{i-1})(Z_i+Z_{i+1})}; \quad (8)$$

$$Z(d_{i-1}) = Z_i \frac{Z(d_i)\cos(k_{xi}d_i)+jZ_i\sin(k_{xi}d_i)}{jZ(d_i)\sin(k_{xi}d_i)+Z_{i+1}\cos(k_{xi}d_i)}; \quad (9)$$

$$Z(d_{N-1}) = Z_0, \quad (10)$$

where k is the wave vector; $k = \beta - j\alpha$, $k = -j\gamma$; Z_i is the characteristic impedance of the i-layer material $Z_i = \sqrt{\frac{j\omega\mu_i}{\sigma_i}}$ (Ω); σ_i is the electrical conductivity of the i-layer material; d_i is the thickness of the i-layer material (m).

According to the microstructure of LZ91/Al Multi-layered composite materials and ignoring α-Mg and β-Li microstructure in LZ91 alloy, then the macroscopic electromagnetic shielding model of $AARB_1$ of Al/LZ91/Al/LZ91/Al is established as shown in Fig. 4.

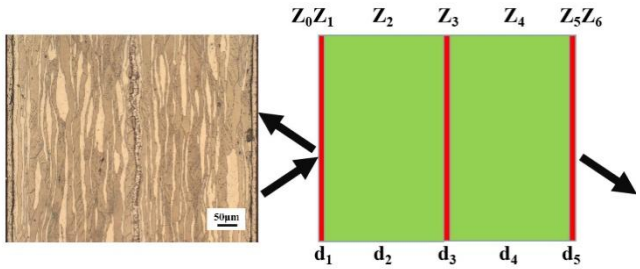

a b

Fig. 4. Electromagnetic shield model of $AARB_1$: a – microstructure; b – electromagnetic shield model

Approximatively consider that the material deforms uniformly in AARB, so, $d_1=d_3=d_5$, $\delta_1=\delta_3=\delta_5$; $d_2=d_4$, $\delta_2=\delta_4$, $Z_6=Z_0$, $Z_1=Z_3=Z_5$, $Z_2=Z_4$. Its mathematical expression of electromagnetic shielding effectiveness is as Eq. 11 – Eq. 13.

$$SE_{A1} = 20\log_{10}\left(e^{\frac{d_1}{\delta_1}+\frac{d_2}{\delta_2}+\frac{d_3}{\delta_3}+\frac{d_2}{\delta_2}+\frac{d_4}{\delta_4}+\frac{d_5}{\delta_5}}\right) = 8.686(3\frac{d_1}{\delta_1} + 2\frac{d_2}{\delta_2}); \quad (11)$$

$$SE_{R1} = -20\log|P| = (20\log_{10}\frac{\left|1+\frac{Z_1}{Z_0}\right|}{2} + 20\log_{10}\frac{\left|1+\frac{Z_0}{Z_1}\right|}{2}) + 2(20\log_{10}\frac{\left|1+\frac{Z_2}{Z_1}\right|}{2} + 20\log_{10}\frac{\left|1+\frac{Z_1}{Z_2}\right|}{2}); \quad (12)$$

$$SE_{B1} = 20\log_{10}|1-q_1e^{-2\alpha_1d_1}| + 20\log_{10}|1-q_2e^{-2\alpha_2d_2}| + 20\log_{10}|1-q_3e^{-2\alpha_3d_3}| + 20\log_{10}|1-q_4e^{-2\alpha_4d_4}| + 20\log_{10}|1-q_5e^{-2\alpha_5d_5}|. \quad (13)$$

The calculation formula of electromagnetic shielding effectiveness of single-layer LZ91 alloy is shown in the introduction, and in the 50 % reduction $AARB_1$ experiment, $t_s = 3d_1 + 2d_2$. And the change of electrical conductivity of LZ91 and Al alloy is ignored during rolling, $\delta_2 = \delta_s$. So compared with LZ91 single-layered alloy, the SE_A increment of $AARB_1$ is expressed as Eq. 14:

$$\Delta SE_{A1} = SE_{A1} - SE_{A0} = 8.686 \times 3d_1(\frac{1}{\delta_1} - \frac{1}{\delta_2}). \quad (14)$$

In Eq. 14, $\sigma_1 > \sigma_2$, so $\delta_1 < \delta_2$, $(\frac{1}{\delta_1} - \frac{1}{\delta_2}) > 0$, then the value of ΔSE_{A1} is positive, meanwhile, $3d_1$ represents the total thickness of Al layer, so for $AARB_1$~$AARB_4$, due to the increase of the Al layer total thickness continuously, thus SE_A increases continuously with the increase of AARB passes.

And due to Z_0=377Ω, Z_1, $Z_2 << Z_0$, and $\frac{Z_2}{Z_1} = \frac{\sqrt{\sigma_1}}{\sqrt{\sigma_2}}$, so the SE_R increment of $AARB_1$ can be expressed as Eq. 15:

$$\Delta SE_{R1} = SE_{R1} - SE_{R0} = 20\log_{10}\frac{Z_2}{Z_1} + 2\left(20\log_{10}\frac{\left|2+\frac{Z_2}{Z_1}+\frac{Z_1}{Z_2}\right|}{4}\right). \quad (15)$$

In Eq. 15, $20\log_{10}\frac{Z_2}{Z_1}$ is SE_R increment of the surface reflective surface which caused by changing LZ91 to Al alloy. $2\left(20\log_{10}\frac{\left|2+\frac{Z_2}{Z_1}+\frac{Z_1}{Z_2}\right|}{4}\right)$ is SE_R increment due to the change of the number of inner layers. And $\sigma_1 > \sigma_2$, $\frac{Z_2}{Z_1} > 1$, $\frac{\left|2+\frac{Z_2}{Z_1}+\frac{Z_1}{Z_2}\right|}{4} > 1$, then the value of ΔSE_{R1} is positive.

As for $AARB_n$ (n is the AARB pass), the SE_R increment is shown as Eq. 16.

$$\Delta SE_{Rn} = 20\log_{10}\frac{Z_2}{Z_1} + 2^n\left(20\log_{10}\frac{\left|2+\frac{Z_2}{Z_1}+\frac{Z_1}{Z_2}\right|}{4}\right). \quad (16)$$

It can be seen that the coefficient of $20\log_{10}\frac{\left|2+\frac{Z_2}{Z_1}+\frac{Z_1}{Z_2}\right|}{4}$ corresponds to the number of LZ91 alloy layers in each pass in Eq. 16. Thus for the multi-layered LZ91/Al composite materials, due to the replacement between LZ91 alloy and Al alloy on the surface and the superposition of heterogeneous metals, the SE_R is increased. Besides, with the increase of AARB passes, the SE_R increases sharply because of the sharp increase of heterogeneous metals stacking.

And the SE_B increment of $AARB_1$ can be expressed as Eq. 17:

$$\Delta SE_{B1} = SE_{B1} - SE_{R0} = \left(2\times 20\log_{10}\left|1-\frac{(Z_1-Z_0)(Z_1-Z_2)}{(Z_1+Z_0)(Z_1+Z_2)}e^{-\frac{2d_1}{\delta_1}}\right| - 20\log_{10}\left|1-\frac{(Z_2-Z_0)^2}{(Z_2+Z_0)^2}e^{-\frac{2t_S}{\delta_2}}\right|\right) + \left(2\times 20\log_{10}\left|1-\frac{(Z_2-Z_1)^2}{(Z_2+Z_1)^2}e^{-\frac{2d_2}{\delta_2}}\right| + 20\log_{10}\left|1-\frac{(Z_2-Z_1)^2}{(Z_2+Z_1)^2}e^{-\frac{2d_1}{\delta_1}}\right|\right). \quad (17)$$

In Eq. 17, when the electromagnetic wave is at the low frequency, $\delta >> d$, $e^{\frac{d}{\delta}} = 1$, then Eq. 17 can be rewritten as Eq. 18:

$$\Delta SE_{B1} = 2\times 20\log_{10}\left|\frac{2Z_2}{(Z_1+Z_2)}\right| - 20\log_{10}\left|4\frac{Z_2}{Z_0}\right| + 2\times 20\log_{10}\left|\frac{4Z_1Z_2}{(Z_2+Z_1)^2}\right| + 20\log_{10}\left|\frac{4Z_1Z_2}{(Z_2+Z_1)^2}\right| = 20\log_{10}\left|\frac{\left(\frac{2Z_2}{(Z_1+Z_2)}\right)^2\left(\frac{4Z_1Z_2}{(Z_2+Z_1)^2}\right)^3}{4\frac{Z_2}{Z_0}}\right|. \quad (18)$$

In Eq. 18, $Z_0 >> Z_1$、Z_2, $\frac{\left(\frac{2Z_2}{(Z_1+Z_2)}\right)^2\left(\frac{4Z_1Z_2}{(Z_2+Z_1)^2}\right)^3}{4\frac{Z_2}{Z_0}}$ is greater than 1, then the value of ΔSE_{B1} is positive.

While the electromagnetic wave is at the high frequency, $\delta << d$, $20\log_{10}|1-q_1e^{-2\alpha_1 d_1}| = 20\log_{10}\left|1-q_1\left(cos4\pi\frac{d_2}{\delta_2}-jsin4\pi\frac{d_2}{\delta_2}\right)\right| = 20\log_{10}|1+q_1|$, so its SE_B increment can be rewritten as Eq. 19:

$$\Delta SE_{B1} = 20\log_{10}\left|\frac{|1+q_1||1+q_2||1+q_3||1+q_4||1+q_5|}{|1+q|}\right| = 20\log_{10}\left|\frac{\left(\frac{2Z_2}{(Z_1+Z_2)}\right)^2\left(\frac{2\left(Z_2{}^2+Z_1{}^2\right)}{(Z_2+Z_1)^2}\right)^3}{2}\right|. \quad (19)$$

In Eq. 19, $\left|\frac{\left(\frac{2Z_2}{(Z_1+Z_2)}\right)^2\left(\frac{2\left(Z_2{}^2+Z_1{}^2\right)}{(Z_2+Z_1)^2}\right)^3}{2}\right| > 1$ by calculation, so the value of ΔSE_{B1} is positive. In sum, the SE_B of $AARB_1$ is higher than that of LZ91 in all frequencies.

As for $AARB_n$, the SE_B increment is shown as Eq. 20 and Eq. 21.

At the low frequency:

$$\Delta SE_{Bn} = 20\log_{10}\left|\frac{\left(\frac{2Z_2}{(Z_1+Z_2)}\right)^2\left(\frac{4Z_1Z_2}{(Z_2+Z_1)^2}\right)^{(2^{n+1}-1)}}{4\frac{Z_2}{Z_0}}\right|. \quad (20)$$

At the high frequency:

$$\Delta SE_{Bn} = 20\log_{10}\left|\frac{\left(\frac{2Z_2}{(Z_1+Z_2)}\right)^2\left(\frac{2\left(Z_2{}^2+Z_1{}^2\right)}{(Z_2+Z_1)^2}\right)^{(2^{n+1}-1)}}{2}\right|. \quad (21)$$

In Eq. 20 and Eq. 21, the index of $\left(\frac{2Z_2}{(Z_1+Z_2)}\right)$ is 2, which represents the two surface layers of multi-layered LZ91/Al composite materials. And the index values of $\left(\frac{4Z_1Z_2}{(Z_2+Z_1)^2}\right)$ and $\left(\frac{2\left(Z_2{}^2+Z_1{}^2\right)}{(Z_2+Z_1)^2}\right)$ represent the number of internal layers of multi-layered LZ91/Al composite materials, it is equal to the sum of the total number of LZ91 layer and Al layer minus 2. The calculations show that the value of $\left(\frac{4Z_1Z_2}{(Z_2+Z_1)^2}\right)$ is always less than 1, that is, while *n* goes to infinity, the value of $\left(\frac{4Z_1Z_2}{(Z_2+Z_1)^2}\right)^{(2^{n+1}-1)}$ goes to zero, so the SE_B increment gradually turns from positive to negative with the increase of pass at the low frequency, but for $AARB_1$~$AARB_4$, their increments are positive, which represents that their SE_B increase in AARB. the value of $\left(\frac{2\left(Z_2{}^2+Z_1{}^2\right)}{(Z_2+Z_1)^2}\right)$ is always greater than 1, which represents that their SE_B increase with the increase of pass at the high frequency. However, at 1300 MHz~1500 MHz, the electromagnetic shielding effectiveness of $AARB_2$ is slightly lower than that of $AARB_1$, and its value is different from the calculation results, which may be caused by its tissue defects or other reasons. This phenomenon needs to be verified by further research, which will be the focus of our follow-up research.

4. CONCLUSIONS

1. AARB can prepare the multi-layered LZ91/Al composite materials as Al/Mg/Al/Mg/...Al, the number of layers of LZ91 and Al alloy increases exponentially and the layer thickness decreases uniformly during each pass. And AARB can also refine grains, after $AARB_4$, most of the α-Mg in ND are refined to less than 1 μm. Besides, α-Mg and β-Li alternate evenly in the interior of the multi-layered LZ91/Al composite materials.
2. The multi-layered LZ91/Al composite materials have excellent electromagnetic shielding effectiveness, and their values are all greater than 100 dB. Due to the increase of the total thickness of the Al layer and the sharp increase of the layer number and interface of LZ91/Al heterogeneous metals, so the electromagnetic shielding effectiveness generally increases with the increase of AARB passes , and the phase interface of α-Mg/β- Li also has a certain influence.

REFERENCES

1. **Wu, X.Y., Han, B.Y., Zhang, H.B., Xie, X., Tu, T.X., Zhang, Y., Dai, Y., Yang, R., Yu, Z.Z.** Compressible, Durable and Conductive Polydimethylsiloxane-coated MXene Foams for High-performance Electromagnetic Interference Shielding *Chemical Engineering Journal* 381 2020: pp. 122622 – 122630. https://doi.org/10.1016/j.cej.2019.122622
2. **Guo, Y., Jian, X., Zhang, L., Mu, C.H., Yin, L.J., Xie, J.L., Mahmood, N., Dou, S.H., Che, R.C., Deng, L.J.** Plasma-induced FeSiAl@Al2O3@SiO2 Core–shell Structure for Exceptional Microwave Absorption and Anti-oxidation at High Temperature *Chemical Engineering Journal* 384 2020: pp. 123371 – 123378. https://doi.org/10.1016/j.cej.2019.123371
3. **Al Naim, A.F., Ibrahim, S.S., El-Shamy, A.G.** A New Class of Electromagnetic Shields Based on Carbon Dots Adorning Te Nanorods Embedded into PEDOT:PSS for Protection from Electromagnetic (EM) Pollutions *Progress in Organic Coatings* 161 2021: pp. 106509 – 106521. https://doi.org/10.1016/j.porgcoat.2021.106509
4. **Chen, X.J., Liu, H.Y., Hu, D.C., Liu, H.Q., Ma, W.S.** Recent Advances in Carbon Nanotubes-based Microwave Absorbing Composites *Ceramics International* 47 (17) 2021: pp. 23749 – 23761. https://doi.org/10.1016/j.ceramint.2021.05.219
5. **Pal, R., Goyal, S.L., Rawal, I., Asha.** Lightweight Graphene Encapsulated with Polyaniline for Excellent Electromagnetic Shielding Performance in X-band (8.2–12.4 GHz) *Materials Science and Engineering: B* 270 2021: pp. 115227 – 115241. https://doi.org/10.1016/j.mseb.2021.115227.
6. **Aal, N.A., El-Tantawy, F.M., Hajry, A., Bououdina, M.** New Antistatic Charge and Electromagnetic Shielding Effectiveness from Conductive Epoxy Resin/Plasticized Carbon Black Composites *Polymer Composites* 29 (2) 2010: pp. 125 – 132. https://doi.org/10.1016/10.1002/pc.20334
7. **Chen, Y., Li, J.Z., Li, T., Zhang, L.K., Meng, F.B.** Recent Advances in Graphene-based Films for Electromagnetic Interference Shielding: Review and Future Prospects *Carbon* 180 (4) 2021: pp. 163 – 184. https://doi.org/10.1016/j.carbon.2021.04.091

8. **Liu, L.Z., Chen, X.H., Pan, F.S.** A Review on Electromagnetic Shielding Magnesium Alloys *Journal of Magnesium and Alloys* 9(6) 2021: pp. 1906 – 1921. https://doi.org/10.1016/j.jma.2021.10.001
9. **Liu, L.Z., Chen, X.H., Wang, J.F., Qiao, L.Y., Gao, S.Y., Song, K., Zhao, C.Y., Liu, X.F., Zhao, D., Pan, F.S.** Effects of Y and Zn Additions on Electrical Conductivity and Electromagnetic Shielding Effectiveness of Mg-Y-Zn Alloys *Journal of Materials Science & Technology* 35 (6) 2018: pp. 1074 – 1080. https://doi.org/10.1016/j.jmst.2018.12.010
10. **Liu, L.Z., Chen, X.H., Wang, J.F., Tang, A.T., Wang, X.L., Liu, J., Gao, S.Y.** Microstructure, Texture, Mechanical Properties and Electromagnetic Shielding Effectiveness of Mg–Zn–Zr–Ce Alloys *Materials Science and Engineering: A* 669 2016: pp 259 – 268. https://doi.org/10.7666/d.d129687
11. **Chen, X.H., Liu, J., Zhang, Z.H., Pan, F.S.** Effect of Heat Treatment on Electromagnetic Shielding Effectiveness of ZK60 Magnesium Alloy *Materials & Design* 42 2012: pp. 327 – 333. https://doi.org/10.1016/j.matdes.2012.05.061
12. **Wang, J.H., Wu, R.Z., Feng, J., Hou, L.G., Zhang, M.L.** Influence of Rolling Strain on Electromagnetic Shielding Property and Mechanical Properties of Dual-phase Mg-9Li Alloy *Materials Characterization* 157 2019: pp. 109924 – 109931. https://doi.org/10.1016/j.matchar.2019.109924
13. **Xu, Z.C., Feng, Z.X., Shi Q.N., Yang Y.X., Wang X.Q..** The Microstructure of Mg 98.5 Zn 0.5 Y 1 Alloy with Long-Period Stacking Ordered Structure *Materials Transactions* 58(06) 2017: pp. 862 – 867. https://doi.org/10.2320/matertrans.M2016440]
14. **Schulz, R.B., Plantz, V.C., Brush, D.R.** Shielding Theory and Practice *IEEE Transactions on Electromagnetic Compatibility* (30) 3 1988: pp. 187 – 201. https://doi.org/10.1109/15.3297
15. **Roghani, H., Borhani, E., Shams, S.A.A., Lee, C.S., Jafarian, H.R.** On the Microstructure, Texture and Mechanical Properties Through Heat Treatment in Al–CuO Nanocomposite Fabricated by Accumulative Roll Bonding (ARB) *Materials Science and Engineering: A* 2021: pp. 142080 – 142089. https://doi.org/10.1016/j.msea.2021.142080
16. **Magalhães, D.C.C, Cintho, O.M., Rubert, J.B., Sordi, V.L., Kliauga, A.M.** The Role of Shear Strain During Accumulative Roll-Bonding of Multilayered Composite Sheets: Pattern Formation, Microstructure and Texture Evolution *Materials Science and Engineering: A* 796 2020: pp. 140055 – 140071. https://doi.org/10.1016/j.msea.2020.140055
17. **Ji, Q., Ma, Y.J., Wu, R.Z., Zhang, J.H., Hou, L.G., Zhang, M.L.** Effect of Y and Ce Addition on Microstructures and Mechanical Properties of LZ91 Alloys *Journal of Alloys and Compounds* 800 2019: pp. 72 – 80. https://doi.org/10.1016/j.jallcom.2019.06.003
18. **LeBozec, N., Thierry, D., Persson, D., Riener, C.K., Luckeneder, G.** Influence of Microstructure of Zinc-Aluminium-Magnesium Alloy Coated Steel on the Corrosion Behavior in Outdoor Marine Atmosphere *Surface and Coatings Technology* 374 2019: pp. 897 – 909. https://doi.org/10.1016/j.surfcoat.2019.06.052
19. **Nie, J.K., Wang, G.K., Hou, D., Guo, F., Han, Y.** The Preparation and Research on the Electromagnetic Shielding Effectiveness of T-ZnO@Ag/Silicone Rubber Composites 22(4) *Materials Science (Medžiagotyra)* 26 (2) 2019: pp. 205 – 209. https://doi.org/10.5755/j01.ms.26.2.21286
20. **Yao, C., Li, J.Z., Li, T., Zhang, L.K., Meng, F.B.** Recent Advances in Graphene-based Films for Electromagnetic Interference Shielding: Review and Future Prospects *Carbon* 180 2021: pp. 163 – 184. https://doi.org/10.1016/j.carbon.2021.04.091
21. **Gao, R., Jin, M., Han, F., Wang, B.M., Wang, X.P., Fang, Q.F., Dong, Y.H., Sun, C., Shao, L., Li, M.D., Li, J.** Superconducting Cu/Nb Nanolaminate by Coded Accumulative Roll Bonding and Its Helium Damage Characteristics *Acta Materialia* 197 2020: pp. 212 – 223. https://doi.org/10.1016/j.actamat.2020.07.031
22. **Abukay, D., Rao, K.V., Arajs, S., Yao, Y.D.** Electrical Resistivity of Aluminium-boron Composites Between 78K and 400K *Fibre Science and Technology* 10 (4) 1977: pp. 313 – 318. https://doi.org/10.1016/0015-0568(77)90007-0